Eindhoven University of Technology
Department of Mechanical Engineering
Group of Engineering Dynamics & Biomechanics

Measuring the response of brain tissue model material to transient loading

H.T.E. Folgering

Under supervision of:

Dr.Ir. P.H.M. Bovendeerd
Ir. D.W.A. Brands

Computational and Experimental Engineering

Contents

Chapter 1

Introduction

1.1 Introduction

Mechanically induced trauma to the body is the leading cause of years of life lost to society and head injuries provide the major contribution, particularly with regard to death and disability of the younger age group. In urban centres of developing countries, trauma morbidity may surpass the contributions of all other diseases, particularly due to motor vehicle crashes. Biomechanics therefore, is becoming, along with the more traditional sciences of biology and chemistry, one of the foundational bases of modern medicine.

One of the earliest rational approaches to the understanding of the mechanics of brain trauma was by the physicist Holbourn in Oxford, who, in 1943 wrote: "Damage to the brain is a consequence, direct or indirect, of the movements, forces and deformations at each point in the brain. The movements, forces and deformations are not independent; so it is sufficient to express everything in deformations. These are worked out with strict adherence to Newton's Laws of Motion, but with approximations to the constitution and shape of the skull and brain. Hence further advances can only come by making better approximations." Holbourn built and tested half-head physical models using gelatin as a brain simulating material and confirmed the relative weakness of gelatin under shearing and tensile loads as compared to its strength when subjected to pure compressive loads. These models were subjected to angular and linear displacements and it was only under the former condition that the higher strains in zones where brain lesions were known to occur were indeed observed in this model. These pioneering model studies provided a good source for explanations of contemporaneous clinicopathologic studies in human head injuries and in experimental animal models also carried out at Oxford in that decade, which suggested that dynamic loading of the head (impact) was necessary to cause traumatic unconsciousness.

However, Holbourn's predictions "ex hypothesis" were not directly tested until much later. At about the same time in the U.S.A., Gurdijan, Lissner, Haynes, Webster, Evans and others working in Detroit carried out the first experimental studies on skull fracture mechanisms using cadavers. These investigations also sought to relate intracranial pressure changes to measurements of head acceleration using linear accelerometers. This work lead to the Wayne State curve for head injury tolerance, which formed the

basis of the work of C. Gadd, who with others, developed the engineering requirements for a head injury criterion (H.I.C.) [2].

1.2 Objectives

At the Eindhoven University of Technology (TUE) a PhD project is running, called: "Determining the dynamic behaviour of brain tissue due to impact loading". In this project it is assumed that an external load on the head (for example during a traffic accident) will lead to a local response of the brain tissue in the head. This local response is, in turn, responsible for the resulting injury. This means that it is necessary to find a relationship between external loading of the head and the local response of brain tissue in the head. Figure 1.1 would be a typical example of a so-called load-injury model.

It is, however, impossible to determine this local response *in-vivo* during impact loading, characteristically lasting about 10 milliseconds. That is why numerical head models are being developed, for example by means of Finite Element Modelling. Verification of these numerical models takes place using physical models. Here, a head is simulated with an experimental set-up consisting of technical (non-biologic) materials. These experimental head models can also be used to approximate which mechanical phenomenons will occur in the head during impact loading.
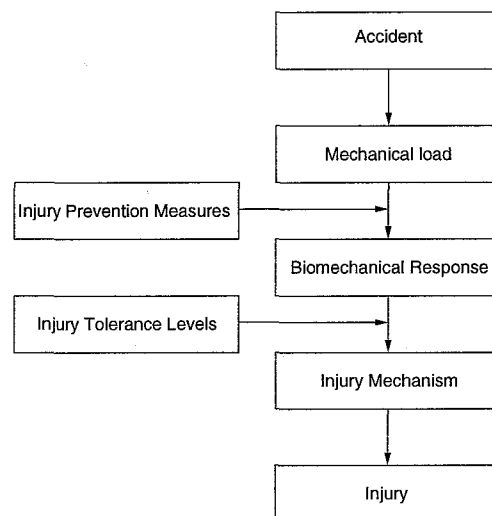
Figure 1.1: The load/injury model [3]

At the TNO Institute of Applied Physics (TNO-TPD) extensive research was done into, what is called, "blunt trauma measuring systems" and ways of measuring the propagation of transient waves in gelatine. Findings there were that qualitative optical measurements are very well possible, however no quantitative data were obtained. Several pressure gauges were used to monitor wave propagation [4] [5].

In the Biomechanics Laboratory of the Mechanical Engineering Department of the TUE a set-up is present, with which by means of a high-speed video camera and markers, *the dynamic response of a brain tissue model material under transient rotational loading* can be made visible [6].

The objective of this traineeship is to assess the possibilities of the above set-up to analyse *the dynamic response of brain tissue model material to transient loading*. Emphasis is laid on the propagation of dilatational waves in brain tissue model material. Topics investigated are:

- Exploration of the boundaries of the high speed camera, as it is taken to the limits of its performance. The camera has a limited frame rate, even for low resolution images.

- Application of the load to produce dilatational waves.

- Analysis of the manner in which the model material reacts to different types of loading.

Chapter 2

Theory: Wave propagation in solids

2.1 Introduction

In this chapter the equations of motion of an isotropic elastic medium will be derived in terms of the particle displacements, and it will be shown that these equations of motion correspond to two types of waves which can be propagated through an extended elastic solid. These two types of waves are termed *dilatational* and *distortional*.
If the solid is unbounded these are the only two types of waves which can be propagated through it. When the solid has a free surface or where there is a surface boundary between two solids, Rayleigh surface waves may also be propagated; these are discussed later in the chapter.

2.2 Types of elastic waves

The most common types of elastic waves in solids are [8]:

1. *dilatational (compression) waves.* In infinite and semi-infinite media, these are known as *longitudinal* waves. These waves correspond to the motion of the particles back and forth along the direction of wave propagation such that the particle velocity is parallel to the wave velocity. If the wave is compressive, they have the same sense; if it is tensile, they have opposite senses.

2. *distortional (shear, transverse) waves.* The motion of the particles conveying the wave are perpendicular to the direction of the propagation of the wave itself, i.e. in the direction parallel to the wave front.

3. *surface (Rayleigh) waves.* This type of wave is restricted to the region adjacent to the surface. The particles on the surface describe elliptical trajectories as the wave moves by. Surface waves (called Rayleigh waves in solids) are a particular case of interfacial waves when one of the materials has negligible density and elastic wave velocity.

Lord Rayleigh suggested that since these surface waves spread only in two dimensions and consequently fall off more slowly with distance than elastic body waves, they might

be expected to be of importance to seismic phenomena. This is, in fact, largely borne out by the seismographic records of the waves observed some distance away from an earthquake. these records show three separate groups of waves. The first to arrive are waves in which the vibrations are predominantly longitudinal, these being dilatational waves which have the highest propagation velocity. Next come the distortion waves, in which the motion is found to be mainly transverse, and the third group is of surface waves whose amplitude is large compared with that of the other two.

If this last group consisted of pure Rayleigh waves, it should have both vertical and horizontal components, the former predominating. This is not in practice found to be the case, the vertical component sometimes being completely absent. For Rayleigh waves the direction of vibration of the horizontal components should be parallel to the direction of propagation, whereas horizontal components parallel to the wave front are often found. Love (1911) has suggested that these waves can be accounted for by assuming that the elasticity and the density of the outer layer of the earth differs from that in the interior [7].

2.3   Energy

The surface waves are the slowest of the three waves. The fastest are dilatational waves, as will be seen from the derivations that follow.

The waves decay at different rates. This decay is a matter of geometry; as the wave travels away from its initiation point, it spreads out. The amplitude of the dilatational wave decays more readily close to the surface. The amplitude of the dilatational and distortional waves decay as r^{-1} in the region away from its effect. Along the surface, they decay faster, as r^{-2}. The Rayleigh wave decays much slower, at a rate of $r^{-1/2}$. Thus, it can be picked up at much larger distances. This decay can be shown by strictly energetic arguments. This will not be discussed any further. Most of the energy is carried by the Rayleigh wave (67% for $\nu = 0.25$). the shear wave carries 26% of the energy and the dilatational wave only carries 7% [8].

2.4   Governing equations

The equations for a homogeneous isotropic solid may be summarised in tensor notation as [9]:

$$\vec{\nabla} \cdot \boldsymbol{\sigma} + \rho \vec{f} = \rho \ddot{\vec{u}} \tag{2.1}$$

$$\boldsymbol{\sigma} = \lambda tr(\boldsymbol{\epsilon}) \boldsymbol{I} + 2\mu \boldsymbol{\epsilon} \tag{2.2}$$

$$\boldsymbol{\epsilon} = \frac{1}{2}\{(\vec{\nabla}\vec{u}) + ((\vec{\nabla}\vec{u})^c\} \tag{2.3}$$

$$\boldsymbol{\Omega} = \frac{1}{2}\{((\vec{\nabla}\vec{u})^c - (\vec{\nabla}\vec{u})\} \tag{2.4}$$

where $\boldsymbol{\sigma}$ is the stress tensor at a point and $\vec{u}$ is the displacement vector of a material point taken with respect to the undeformed configuration. The stress tensor is symmetric, so that $\boldsymbol{\sigma} = \boldsymbol{\sigma}^c$. The mass per unit volume of the material is ρ and $\vec{f}$ is the body force per unit mass of material. The infinitesimal, linear strain and rotation tensors are

8

given by ϵ and Ω, respectively. The elastic constants for the material are λ and μ, the Lamé constants. The latter is the shear modulus and both constants may be expressed in terms of the other elastic constants, such as Young's modulus, Poisson's ratio, and the bulk modulus.

The governing equations in terms of the displacements are obtained by substituting the expression for strain (2.3) onto the stress-strain relation (2.2) and the result thereof into the equation of motion (2.1), giving Navier's equation for the media

$$(\lambda + \mu)\vec{\nabla}(\vec{\nabla} \cdot \vec{u}) + \mu\nabla^2\vec{u} + \rho\vec{f} = \rho\ddot{\vec{u}}. \tag{2.5}$$

Using the vector identity

$$\nabla^2\vec{u} = \vec{\nabla}(\vec{\nabla} \cdot \vec{u}) - \vec{\nabla} \times (\vec{\nabla} \times \vec{u}), \tag{2.6}$$

and defining the dilatation Δ of a material by

$$\Delta = \vec{\nabla} \cdot \vec{u} = tr(\epsilon), \tag{2.7}$$

and the rotation vector $\vec{\omega}$ by

$$\vec{\omega} = \frac{1}{2}\vec{\nabla} \times \vec{u}, \tag{2.8}$$

we may express (2.5) as

$$(\lambda + 2\mu)\vec{\nabla}\Delta - 2\mu\vec{\nabla} \times \vec{\omega} + \rho\vec{f} = \rho\ddot{\vec{u}}. \tag{2.9}$$

The dilatation Δ describes the change in volume, while the rotation vector $\vec{\omega}$ represents the shear deformation. One of the advantages of (2.9) is that it explicitly displays the dilatation and rotation.

In future, the body forces will be neglected. This will make the equations of motion homogeneous (i.e. homogeneous differential equations in the displacement $\vec{u}$).

2.5 Dilatational waves

Consider the governing displacement equations (2.5) in the absence of body forces, given by

$$(\lambda + \mu)\vec{\nabla}(\vec{\nabla} \cdot \vec{u}) + \mu\nabla^2\vec{u} = \rho\ddot{\vec{u}}. \tag{2.10}$$

If the vector operation of divergence is performed on the above, we obtain

$$(\lambda + \mu)\vec{\nabla} \cdot (\vec{\nabla}(\vec{\nabla} \cdot \vec{u})) + \mu\vec{\nabla} \cdot (\nabla^2\vec{u}) = \rho\vec{\nabla} \cdot \ddot{\vec{u}}. \tag{2.11}$$

With $\nabla^2 = \vec{\nabla} \cdot \vec{\nabla}$, $\vec{\nabla} \cdot (\nabla^2\vec{u}) = \nabla^2(\vec{\nabla} \cdot \vec{u})$, and $\vec{\nabla} \cdot \vec{u} = \Delta$, the dilatation, (2.11) reduces to

$$(\lambda + 2\mu)\nabla^2\Delta = \rho\frac{\partial^2\Delta}{\partial t^2} \tag{2.12}$$

This we recognise as the wave equation, expressible in the form

$$\nabla^2 \Delta = \frac{1}{c_1^2} \frac{\partial^2 \Delta}{\partial t^2} \tag{2.13}$$

We thus conclude that a change in volume, or dilatational disturbance, will propagate at the velocity

$$c_1 = \left(\frac{\lambda + 2\mu}{\rho} \right)^{\frac{1}{2}}. \tag{2.14}$$

2.6 Distortional waves

We now perform the operation of curl on (2.9) in the absence of body forces. This yields

$$(\lambda + 2\mu)\vec{\nabla} \times (\vec{\nabla}\Delta) - 2\mu\vec{\nabla} \times (\vec{\nabla} \times \vec{\omega}) = \rho\vec{\nabla} \times \ddot{\vec{u}}. \tag{2.15}$$

Since the curl of the gradient of a scalar is zero, the first term on the left is equal to zero. With the vector identity (2.6) the second term on the left can be rewritten as

$$-2\mu\vec{\nabla} \times (\vec{\nabla} \times \omega) = 2\mu\nabla^2\vec{\omega} - 2\mu\vec{\nabla}(\vec{\nabla} \cdot \vec{\omega}). \tag{2.16}$$

Recalling $\vec{\omega} = \frac{1}{2}\vec{\nabla} \times \vec{u}$ we get $\vec{\nabla}(\vec{\nabla} \cdot \vec{\omega}) = \frac{1}{2}\vec{\nabla}[\vec{\nabla} \cdot (\vec{\nabla} \times \vec{u})] = 0$, because $\vec{\nabla} \cdot (\vec{\nabla} \times \vec{u}) = 0$. So

$$2\mu\nabla^2\vec{\omega} = 2\rho\frac{\partial^2\vec{\omega}}{\partial t^2}, \tag{2.17}$$

or

$$\nabla^2\vec{\omega} = \frac{1}{c_2^2} \frac{\partial^2\vec{\omega}}{\partial t^2} \tag{2.18}$$

Thus, distortional (rotational) waves propagate with a velocity

$$c_2 = \sqrt{\frac{\mu}{\rho}} \tag{2.19}$$

Dilatational and distortional waves are the only two types of waves that propagate through an unbounded elastic medium [9].

2.7 Surface waves

The derivation of the surface (Rayleigh) wave equation will not be carried out here; the reader is referred to Kolsky [7]. The surface wave velocity - shear wave velocity ratio κ is

$$\kappa = \frac{c_s}{c_2}, \tag{2.20}$$

10

κ can be expressed in ν, resulting in the following relationship between c_s and c_2:

$$c_s = \frac{0.862 + 1.14\nu}{1 + \nu} c_2 \tag{2.21}$$

For a virtually elastic material, Poisson's ratio ν will take on a value rather close to 0.5. For $\nu \to 0.5$, κ will assume a value of 0.95.

Substituting Equation (2.19) in (2.20) gives an expression for the surface wave velocity:

$$c_s = \kappa \sqrt{\frac{\mu}{\rho}} \tag{2.22}$$

11

Chapter 3

Experimental design

3.1 Introduction

A setup is devised to acquire quantitative information from transient loading of brain tissue model material. Roersma [6] assembled it to conduct rotational loading experiments. It is modified to accommodate for impact loading experiments. The setup consists of three major parts; a cup to hold a sample of the model material, a pendulum to inflict an impulse on the cup and a camera to register the response to this impulse. The camera is attached to an image-recorder and a desktop computer to process the data. A short description of each part follows. Also, see Figure 3.1.
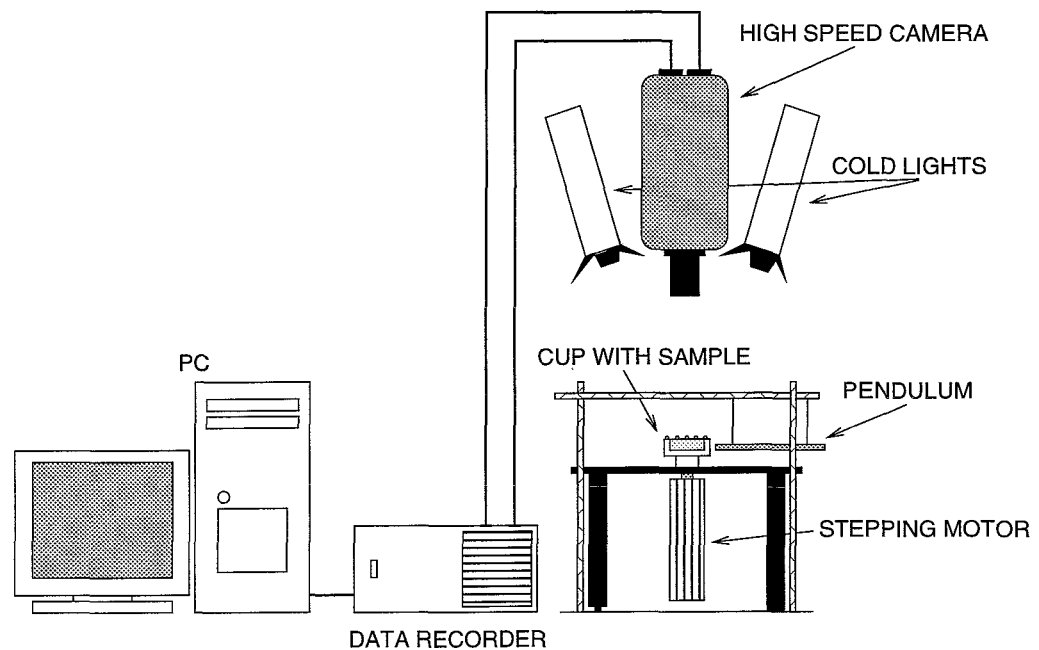

Figure 3.1: The experimental setup

3.2 Experimental setup

3.2.1 The cup and sample material

3.2.1.1 The cup

The cylindrical cup is a simplified model of the human head. It is made of transparent perspex (polymethylmetacrylate, PMMA) and is to hold a sample of gelatine - the brain tissue model material. The cup can contain a volume of 9.2 millilitres ($\pi r^2 h = 3.14 \times (15\text{ mm})^2 \times 13\text{ mm}$), which is about equal to 10 grams of gelatine. It was originally designed and developed for earlier experiments conducted by Roersma [6]. The cup is mounted on a stable table, also used in Roersma's earlier experiments. Both on the rim of the cup as well as in the sample of gelatine it contains, markers are fitted for the high speed camera to register the reaction of the respective media to the pendulum striking the cup. The twelve markers on the rim of the cup are referred to as "world markers". Also, see Figure 3.2.

3.2.1.2 The model material

The gelatine is supplied as a powder by Gelatine Delft N.V. The model material to be contained by the cup is prepared according to a recipe from the TNO Prince Maurits Laboratory in Rijswijk, the Netherlands. Here, research is done for the Dutch Department of Defence in which the gelatine is used as a substitute for human tissue. The recipe is given in Appendix A. In this setup, the sample material has a mass percentage of 4% gelatine, and has stiffened for three to five hours. It is assumed to be fully elastic. It is obvious that the markers in the gelatine should influence the mechanical behaviour of this material as little as possible. For this purpose, small ($\varnothing 2$ mm) polystyrene balls were selected. The density of polystyrene at room temperature is about 1.05 times the density of water at $4°$C. We assume the density of the gelatine to be the same as the density of water. This implies that no additional inertia effects are to be expected due to marker placings. Attaching the markers to the gelatine is done by heating the upper surface of the gelatine (for example by placing it under a hot light bulb) and then carefully arranging the markers on it. When the gelatine restiffens, the markers are fixed in the upper layer of the gelatine. Do note that by reheating the gelatine, it may dry out slightly. This may have effect on the properties of the sample material.
In later experiments, the markers in the gelatine were replaced by small ink dots. Any inertia effects are thus reduced even further. Also, no heating of the gelatine is required this way. A disadvantage of using ink is that it diffuses through the sample material it is put into. Depending on it being water-based or oil-based it will diffuse faster, respectively slower through gelatine.
The markers on or in the sample material are called "object markers".

3.2.2 The pendulum

In the current setup, a steel rod, with length 192 mm, mass 41 grams and diameter 6 mm, is used to impact the cup from the side. It is suspended on two fibrous nylon wires in a steel framework surrounding the cup and the table it is fixed on. When the pendulum is inactive, it is at its lowest point; just touching the outside of the cup.
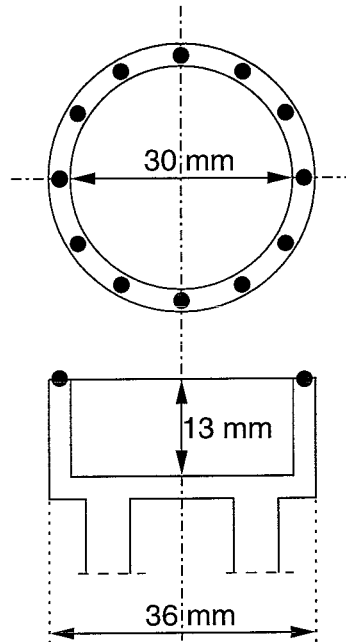
Figure 3.2: Cup and markers

Preparing for impact, the pendulum is lifted to a point 30 mm (± 3 mm) higher than this equilibrium state.

3.2.3 The camera

To record the marker displacement due to impact of the pendulum on the cup, a high speed video camera, type Kodak Ektapro ES Motion Analyser, was used. Its maximum frame rate is 40.500 frames per second (fps). At this rate it produces 8 bit images (256 grey values) of 64×64 pixels [10]. The images are stored in an internal RAM memory and then uploaded to a computer for further processing. At 40.500 fps, the length of time that can be recorded at once is 1.2 seconds. This allows manual synchronising of the release of the pendulum from its elevated state and triggering the recording of the impact.

3.2.4 The stepping motor

Figure 3.1 shows that a stepping motor was present in the setup as well. Again, this has been used in earlier experiments by Roersma. The table to which the stepping motor is fitted, provides enough stability for a solid mounting of the cup. Also, as Roersma's experiments are taken into account during this traineeship, using the same setup as a basis makes it easier to compare the data acquired, as well as having the opportunity to repeat his experiments.

3.2.5 Measurement optimisation

To assure optimal results of the image processing system, three aspects have to be taken into account. Firstly, it is noted that because of the high recording frequency, special
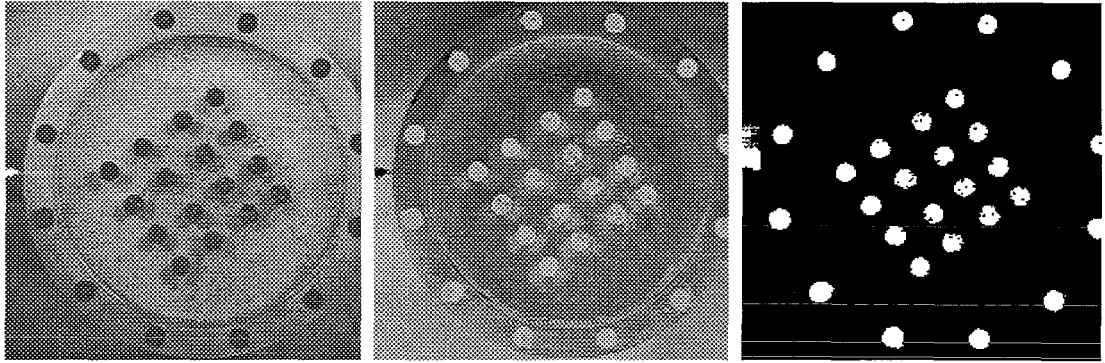
Figure 3.3: An example of thresholding an image. From left to right: (a) the image taken by the camera, (b) the inverted image and (c) the thresholded, inverted image.

lighting equipment should be used. As normal lights also give off a certain amount of heat, this may cause the sample material to dry and change its properties. To avoid this drying of the gelatine when using powerful "flood lights", special "cold lights", which contain an infrared filter, are used in this experiment.

Secondly, the images should be free of reflections and shading. Reflections occur when the light is reflected into the lens of the camera, bouncing off the surface of the sample material. When the cup and its contents are illuminated by diffused light, this problem is avoided. This is done by placing a large cylinder (about Ø12 cm) of plain white paper (80 g/m^2) around the cup. Shading is avoided by using multiple (two) lights.

Thirdly, the contrast between the markers and their surroundings should be as high as possible to enable the image processing system to detect the markers easily. To achieve this, the markers are painted black. In contrast, the table and the bottom of the cup are made white, by means of a sheet of white paper and paint, respectively.

3.3   Image pre-processing

The images acquired from the experiment are pre-processed before actual marker detection takes place, as done by Roersma [6]. After performing the experiment, the recorded images are uploaded to a PC and stored as individual files in general TIFF format. An example of an original image is displayed in Figure 3.3a. The image processing software package TIMWindows (version 1.41.4, 1996) is used to determine the co-ordinates of the markers in every image.

The image is first inverted. The image is stored in 256 different grey values. Grey value (GV) 0 now becomes 255, GV 1 becomes GV 254 etcetera. See Figure 3.3b. The final step of pre-processing is thresholding the inverted image. See Figure 3.3c. Note that apart from the markers, the pendulum is also still present in the image. All grey values below a certain criterion GV$_c$ are set to GV 0 and all grey values above this GV$_c$ are set to GV 255.

3.4 Marker detection

The first image of a recording has to be thresholded manually. The required threshold is determined by visual inspection. If it is chosen too low, noise will be introduced; if it is chosen too high, information may be lost. When one image is pre-processed, TIMWindows is able to identify every white spot in the image as a so-called "object". It can calculate the co-ordinates (in pixels) of the centre of every object. Manually we have to tell the computer which white spot is an actual "object" or marker. This is called marker detection. Other "spots", such as the pendulum can be characterised as "trash". The software used will then automatically load the next image, set it to the same threshold, detect the markers and store the co-ordinates in a file that can be used in Matlab. It will do so for every image. The TIMWindows command files to perform these operations were written by Chris van Oijen, originally by Erwin Noukens and Bas Michielsen, all from Biomechanics Laboratory of the Eindhoven University of Technology, and were modified by Michiel Roersma for use in experiment with rotating cup.

3.5 Expectations

Before acquiring data from the experiment, one must be aware of what is expected to happen as well as of the ability of the monitoring devices to see what will happen. Some limitations of the high speed camera were pointed out in a previous section (3.2.3). Considering the minimum frame size of 64 × 64 pixels, at maximum frame rate, there are limitations to the field of view too. With regard to the displacements of the markers which we would like to measure, the resolution might be a problem.

3.5.1 Dilatational waves

The velocity of dilatational waves through water is 1540 m/s. It is assumed that this is the same through both a 4% and a 20% gelatine solution [5]. The time span between two images at maximum frame rate is 1/40.500 s. During this interval, the dilatational wave traverses $1540/40.500 = 38.0 \times 10^{-3}$ m, say four centimetres. To make sure that we can actually capture a traversing wave in two consecutive frames, we should monitor an area with a width of at least twice that distance, namely eight centimetres. The corresponding frame size would imply a pixel size of $80/64 = 1.25$ mm.

Using Roersma's cup, with an inner diameter of 30 mm, we would never be able to see an induced dilatational wave move through it. Local displacements as a result of this dilatational wave however, may be seen and registered. The question in this case is: will the displacements be significantly larger than the resolution of the high speed camera or than the accuracy with which the centre of the markers can be determined? The former depends on the camera frame rate, the latter depends on the size of the markers used, or more directly; on the number of pixels a marker occupies. The more pixels a marker covers, the more accurately the position of its centre can be determined.

3.5.2 Distortional waves

At 15° Celsius, the shear modulus μ of a 4% gelatine mixture is 7.5 ± 0.5 kPa [11]. The density ρ of the model material is assumed to be the same as that of water: $\rho = 1000$ kg/m^3. Putting these values into Equation (2.19) amounts to an expected distortional wave velocity through gelatine of 2.7 ± 0.1 m/s. This implies that such a wave travels $2.7/40.500 = 67.6 \times 10^{-6}$ m, say 70 μm, between two consecutive frames at maximum camera speed, which is well within range of the size of the cup. When at a recording frequency of 27.000 fps, the wave travels 100 μm in between two frames.

3.5.3 Surface waves

The surface wave velocity can easily be deduced from the distortional wave velocity; see Equations (2.21) and (2.22). Surface waves are expected to travel at 2.6 ± 0.1 m/s through the gelatine mixture.

Chapter 4

Experimental results

4.1 Dilatational waves

To detect dilatational waves, polystyrene marker balls are placed at a level halfway in the sample material. The effect of surface waves is assumed to be negligible here. In later experiments, instead of polystyrene balls, ink dots are used as markers, thus minimising any inertia effects of the markers on the gelatine.

Figure 4.1 represents such an experiment. Figure 4.1a shows the part of the cup that was monitored during the experiment; the area visible is 30 by 30 mm large and the image's resolution is 64 × 64 pixels. Three world markers and five object markers (in this case: ink dots) are visible. The pendulum moves in x-direction and strikes the cup at the the position of World Marker 2. Figure 4.1b and c show the typical responses of a world marker, respectively an object marker to the impact.
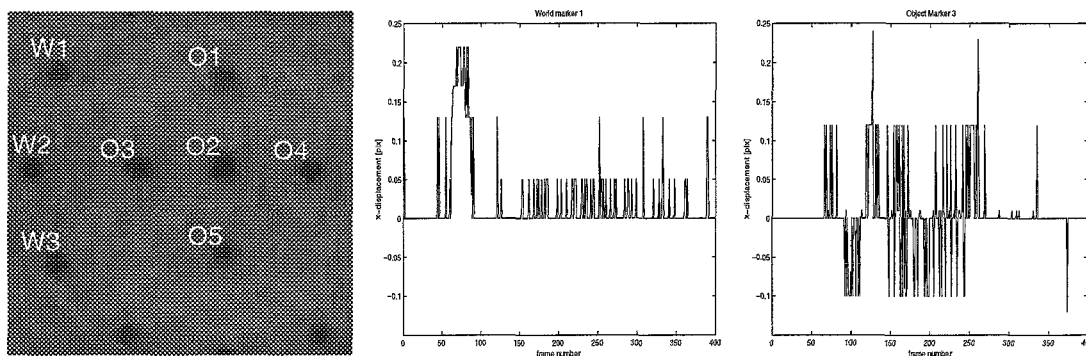

Figure 4.1: Typical impact response of markers. From left to right: (a) a typical image taken by the camera, (b) the displacement in x-direction of World marker no. 1 and (c) the displacement in x-direction of Object marker no. 3.

4.1.1 Accuracy

The experimental setup is not calibrated. Therefore it is not possible to give an exact analysis of the accuracy. It is possible, however, to make some remarks concerning the accuracy of the experiment. The accuracy of the Cartesian co-ordinates in pixels is

determined by the image resolution (64×64 pixels), the marker size and the accuracy of the image processing system. An indication of this accuracy can be obtained by analysing the situation of a non-moving cup. After producing 85 images of a non-moving cup with 4 world markers, the (x,y) co-ordinates of these markers are determined. The results of this are shown below.
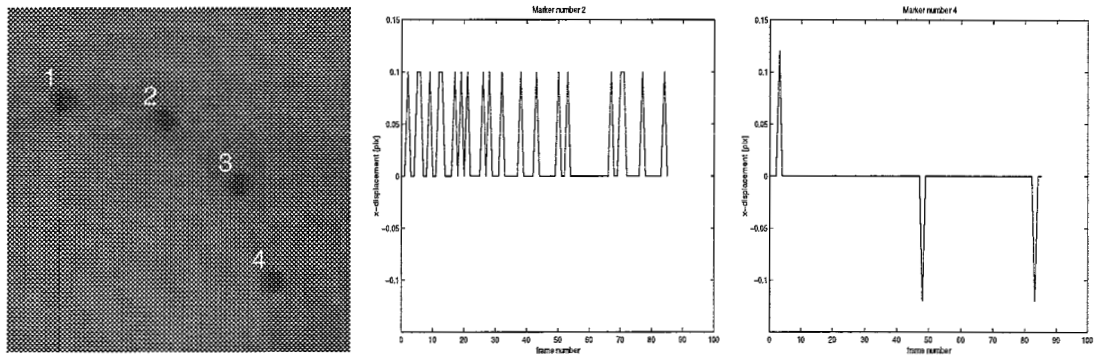

Figure 4.2: Typical characteristics of marker positioning by the data processing software of images of a non-moving cup. Accuracy in y-direction is similar.

4.2 Surface waves

Apart from dilatational waves, impact of the pendulum seems to cause surface waves as well. When polystyrene marker balls are embedded in the surface of the gelatine, these waves can not only be seen with the naked eye, but also through data acquired from monitoring marker displacements.
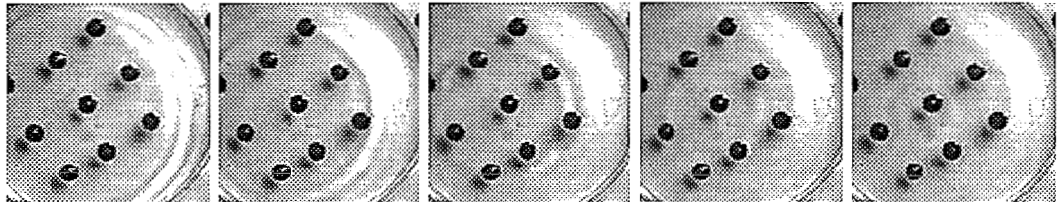

Figure 4.3: Wave propagation through the cup

Figure 4.3 shows, from left to right, a concentric surface wave traversing through the cup from the rim to the centre. In this case only one flood light is used and the paper cylinder diffusing the light is removed. This way any surface waves form shadows on the bottom of the cup which can be picked up by the high speed camera. An additional effect is that part of the waves such as shown in Figure 4.3 reflect off the markers that are fixed on the surface of the gelatine. This is clearly to be seen in video footage of the impact sequence, though not easy to show in still images.

19

Marker displacement is monitored in another trial. In this instance, the frame rate of the high speed camera is dropped to 27.000 fps, which is still high enough to detect surface waves. The frame size now increases to 128×64 pixels. The cup has the polystyrene balls fitted on the surface of the gelatine. Some displacement can be seen, possibly due to surface waves disturbing the markers. This will be discussed in the next chapter. To save time and disk usage, a limited amount of data is stored and processed. Figure 4.4 gives an overview. The pendulum strikes the rim of the cup right between World marker 1 and 2. On the left is the part of the cup that was monitored, on the right typical responses of a world marker and an object marker are shown. More data are presented in Appendix C.
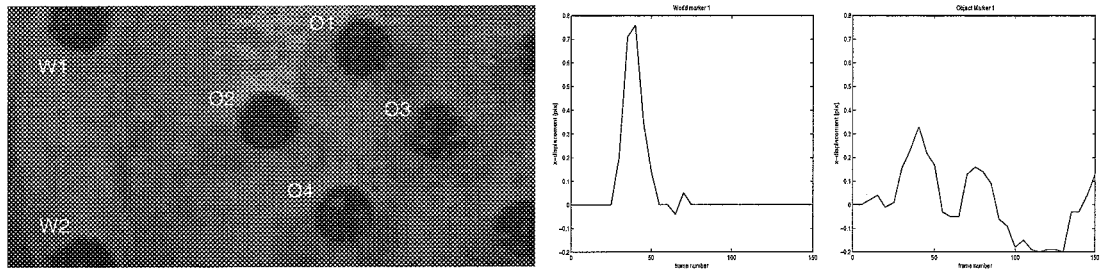

Figure 4.4: Surface marker displacement due to impact

Chapter 5

Discussion

5.1 Impact loading

5.1.1 Dilatational waves

In Figure 4.1 as well as in Appendix B the results of the experiment focusing on dilatational waves are represented. Comparing these with the accuracy measurements in Figure 4.2 and Appendix C, it is difficult to notice any significant marker displacement due to pendulum impact. Though different areas are monitored, both the frame size as well as the image size are the same, respectively 64×64 pixels and 30×30 mm. Appendix C implies an accuracy of one tenth the size of a pixel. The maximum displacement of a marker is thrice as large as this. It is assumed that the peak around frame number 80, which appears in several of the graphs, represents rigid body movement at the time of impact. Apart from this, no marker displacement or traversing wave can bee seen.

Note that in Figure B.2 the data from world marker 2 are distorted as the marker is at the very position where the pendulum strikes the cup. The data processing software assumes world marker 2 and the tip of the pendulum as one object at this time, thus moving the centre of the object away from its initial centre; the centre of the marker. A problem posed by placing markers or ink dots halfway in the gelatine, is that the model material is split in two halves. The gelatine is poured into the cup in two parts; the top half only after the bottom half has stiffened up and the markers are placed on it. The effects of this are neglected in this traineeship. Dow Corning's Sylgard 527 A/B Silicone dielectric gel does merge in this case [12], perhaps it is worthwhile using this for future experiments.

5.1.2 Surface waves

As Figure 4.3 shows, the impact of the pendulum on the cup causes surface waves on the sample material. Obviously, these can only be detected using the methods discussed when markers are present on the surface of the gelatine. Appendix D shows the results. All graphs initially show rigid body movement around frame number 40; see Figures D.2 and D, due to pendulum impact. Then, Figure D shows a peak in the x-displacement of Object Marker 2 at frame number 65, and one in the x-displacement of Object marker 3 at frame number 90. It is assumed that these two peaks are caused by a wave effect,

originated at the time of impact of the pendulum. From these data the velocity of this wave can be determined at 9.5 ± 0.1 m/s. This value is much higher than the theoretical one, determined in Section 3.5.3. The reason for this is not known.

5.2 Rotational loading

Roersma [6] applied a transient rotational loading to the cup by means of a stepping motor, also present in this setup. As a result of this, the gelatine inside the cup deformed. Though the effects are three-dimensional, only the local displacements in the plane of the surface of the gelatine were monitored. The displacements of the markers placed on this surface give an indication of the deformation of the gelatine. Roersma used small polystyrene balls as markers. In Appendix E the marker displacement due to the transient rotation is shown. The high speed camera recorded the images at 4500 frames per second, much slower than the experiments done in this traineeship.

Looking back at Roersma's experiments, they too show signs of surface waves travelling through the cup from the rim towards the centre. Figure 5.1(a) shows a typical response of some of the markers to rotational loading. The fact that inertia effects play a role in the experiments is illustrated in the interval $0 < time < 15$ ms in this figure. It is clear that the angular displacements of the markers are larger in the centre of the cup than near the rim. Besides that, Figure 5.1(a) shows that the oscillations of the object markers are larger than the oscillation of the cup [6].

The inertia effects, or the delay in marker displacements due to surface wave propagation, as they are assumed to be, are further highlighted in Figure 5.1(b). Here, the rotation of the markers is being related to their respective distance away from the centre of rotation.
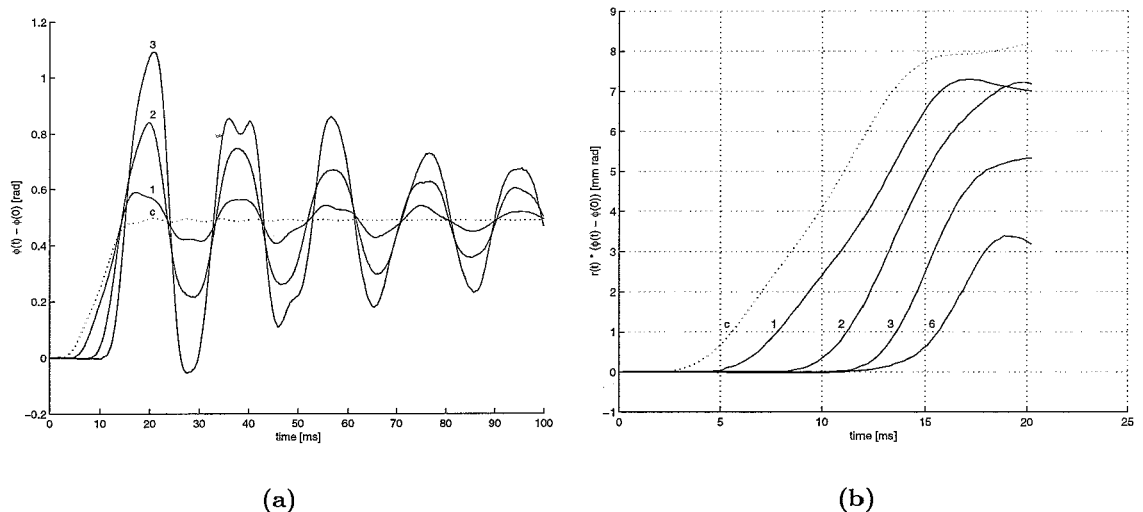

(a)   (b)

Figure 5.1: (a) A typical response to rotational loading. (b) Relating angular displacement to radial position

22

Calculated from the delays in marker displacements in Roersma's results, the average velocity of surface waves during his experiment is: 1.4 ± 0.1 m/s. Although in the same order of magnitude, again the experimental value is significantly less than the theoretical one. The accuracy of the value is based on the fact that the discrete measurement values have to be interpolated in order to fit a curve through the data points on the graph. The data points are each 0.222 seconds apart.

It is not known why this experimental value does not match the theoretical value.

Chapter 6

Conclusions and recommendations

Within one setup, several ways to measure the dynamic response to impact loading of brain tissue model material have been assessed. The setup contained a high speed camera which registered the local displacements within a gelatine-filled cup, after it had been struck by a pendulum. Using results from earlier experiments [6],[11] that were performed in the same laboratory to estimate material parameters of brain tissue, properties of the model material were further researched.

These are some final remarks about what has been found:

6.1 Conclusions

- Dilatational waves travel too fast to be measured within this setup. At maximum frame rate, the camera needs to have a greater field of view to catch a travelling dilatational wave in two consecutive frames. Do note that the resolution of the camera is low at maximum frame rate.

- Surface waves due to impact loading can easily be detected by the high speed camera, even below maximum frame rate, using markers, either polystyrene balls or ink dots, fixed on the surface of the model material.

- Though wave velocities can be quantified, experimental values are some way off the theoretical values.

- Using markers to determine local displacements is suitable for the software used. Applying a grid on or in the model material may improve visual representation of its deformation.

- When the lighting is not diffused and coming from only one direction, the shadows cast on the bottom of the cup by the changes in the surface of the gelatine enhance the visual effect of surface waves, but do not improve the measurements.

- The use of ink dots instead of polystyrene balls as markers relieves the model material of most inertia effects as well as irregularities due to the markers placed in the medium. The material will retain its properties.

24

- Placing markers halfway in the model material used, implies that the gelatine has to be poured into the cup in two parts. These two do not merge into one, which complicates the effects from loading the material. Dow Corning's Sylgard gel does merge in this case, so that might be another reason (see also [11]) to use it in future experiments.

- The behaviour at a free surface of a material is better known than that within the material. Determining the behaviour from the model material using markers fixed on its surface can therefore be more easily be related to theory.

- Though the experiments indicate to be 3-dimensional, 'planar' data give a reasonably good insight into the deformations of the material during the experiments.

- Apart from impact loading, transient rotational loading of the setup used is suitable for doing research on surface wave propagation through a brain tissue model material.

6.2   Recommendations

- Either a camera with a higher recording rate and higher resolution should be used, or a larger area of brain tissue model material should be taken into view to detect dilatational waves travelling through the medium observed.

- A closer look should be taken at the differences in experimental values to theoretical values of distortional and surface waves.

- More research has to be done into the material properties of the model material under transient rotational loading.

Bibliography

[1] ESTC-rapport (1993): *Reducing Traffic Injuries through Vehicle Safety Improvements*, Report of the European Transport Safety Council.

[2] Ommaya, A.K., Thibault, L., and Bandak, F.A. (1994): *Mechanisms of Impact Head Injury*, International Journal of Impact Engineering, Vol. 15, No. 4, pp 535-560, Elsevier Science Ltd., Great Britain.

[3] Wismans, J.S.H.M., et al. (1994): *Injury Biomechanics*, course notes on lecture series, Eindhoven University of Technology, the Netherlands.

[4] Maas, A.A.M., Smorenburg, C., Velzen, G.B.E.M. van (1996): *Voorstudie Blunt Trauma Meetsysteem*, TNO-rapport TPD-HOI-RPT-960003, Delft, the Netherlands.

[5] Smorenburg, C., Velzen, G.B.E.M. van, Moddemeijer, K., Heiden, N. van der, Bree, J.L.M.J. van (1997): *Metingen aan drukgolven in gelatine*, TNO-rapport HOI-RPT-970003, Delft, the Netherlands.

[6] Roersma, M.E. (1998): *Analysis of an experiment to measure the response of soft materials under transient rotational loading*, WFW-report 98.015, Eindhoven University of Technology, the Netherlands.

[7] Kolsky, H. (1963): *Stress Waves in Solids*, Dover Publications, Inc., New York, U.S.A.

[8] Meyers, M.A. (1994): *Dynamic Behaviour of Materials*, John Wiley & Sons, Inc., New York, U.S.A.

[9] Hoof, J.F.A.M. van (1994): *One- and Two-Dimensional Wave Propagation in Solids*, WFW-report 94.055, Eindhoven University of Technology, the Netherlands.

[10] Spee, I. (1997): *User's manual Kodak Ektapro HS Motion Analyser*, WFW-report 97.013, Eindhoven University of Technology, the Netherlands.

[11] Plasmans, C.J.P. (1998): *The dynamical behaviour of a model material for brain tissue*, WFW-report 98.021, Eindhoven University of Technology, the Netherlands.

[12] Viano, D., Aldman, B., Pape, K., Hoof, J. van, Holst, H. van (1997): *Brain kinematics in physical model tests with translational and rotational acceleration*, International Journal of crashworthiness, Vol. 2, No. 2, Woodhead Publishing Ltd., Great Britain.

Appendix A

Preparation of 20% and 4% gelatine mixtures

- Measure off cold water and gelatine grains in a mass ratio of 4:1 or 24:1 , for 20% and 4% gelatine mixtures respectively.

- Add the gelatine grains to the water in a small cup.

- Let the mixture soak and expand for about 45 minutes.

- Put the fluid in a warm bath and heat it up to about 50° Celcius.

- When a clear transparent fluid has formed, it can be poured into the final form, e.g. the cup.

- Remove any possible bubbles (ultrasonically).

- Seal the cup (air-tight) and let the mixtue cool down gently.

- Place the cup in a refrigirator, peferably at 10° Celcius.

- Keep the samples cooled as long as possible and do not remove them from the refrigirator until just before the experiment.

- Preferable testing temperature is 10° Celcius.

From [11].

Appendix B

Dilatational waves
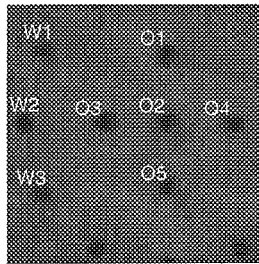
Figure B.1: The area of the cup that was monitored during impact (image size: 64×64)
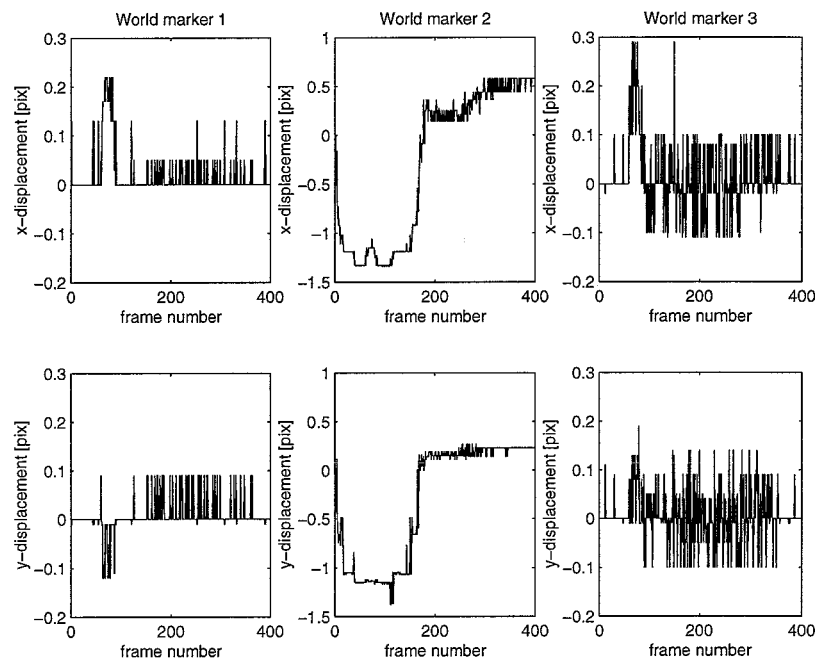
Figure B.2: World marker displacement
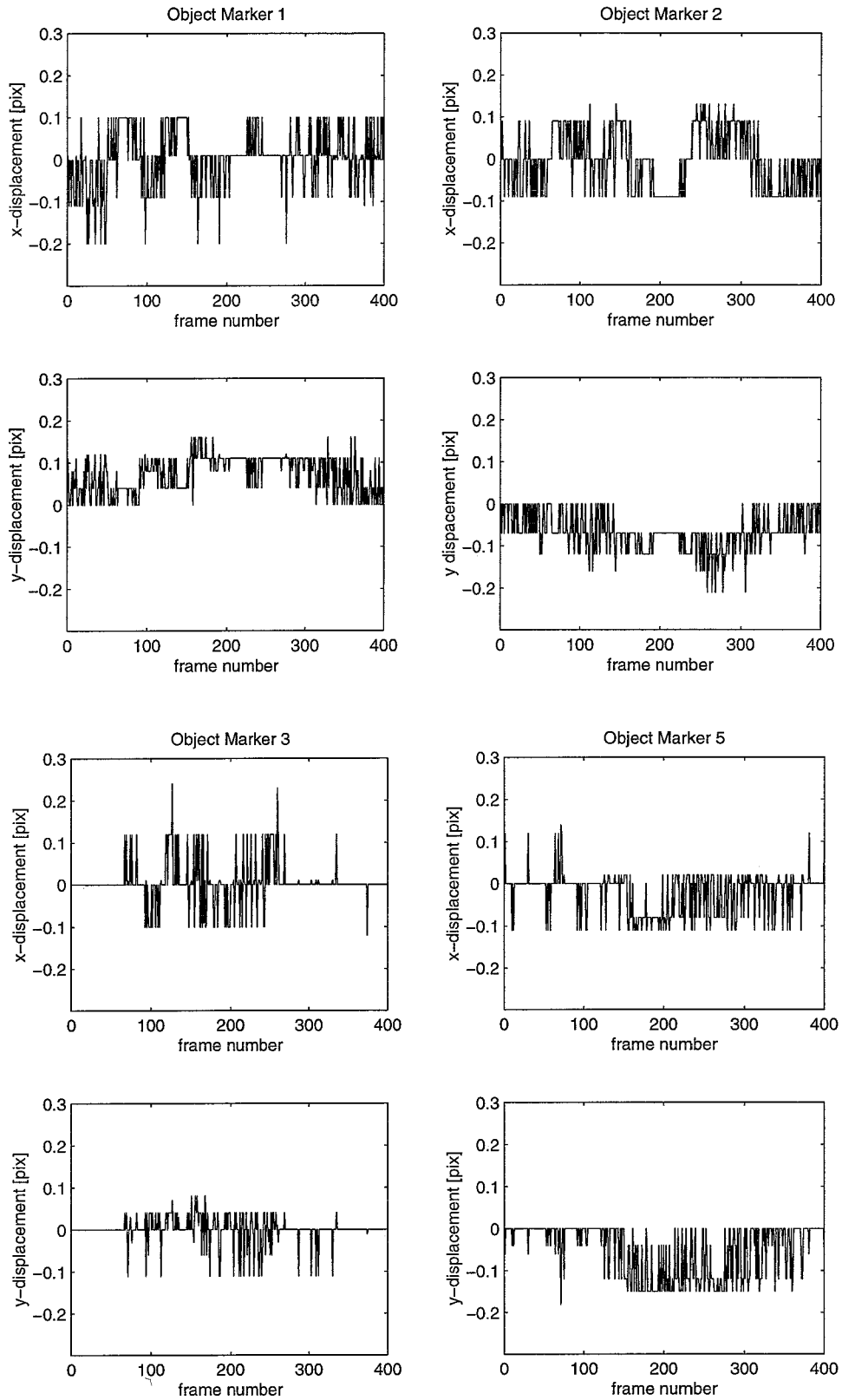
Figure B.3: Object marker displacement

Appendix C

Accuracy measurements
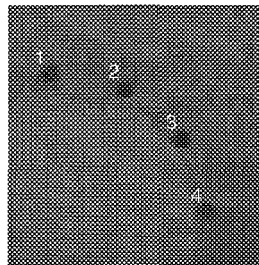
Figure C.1: An image from the series of 85 of the non-moving cup (frame size: 64×64 pixels)
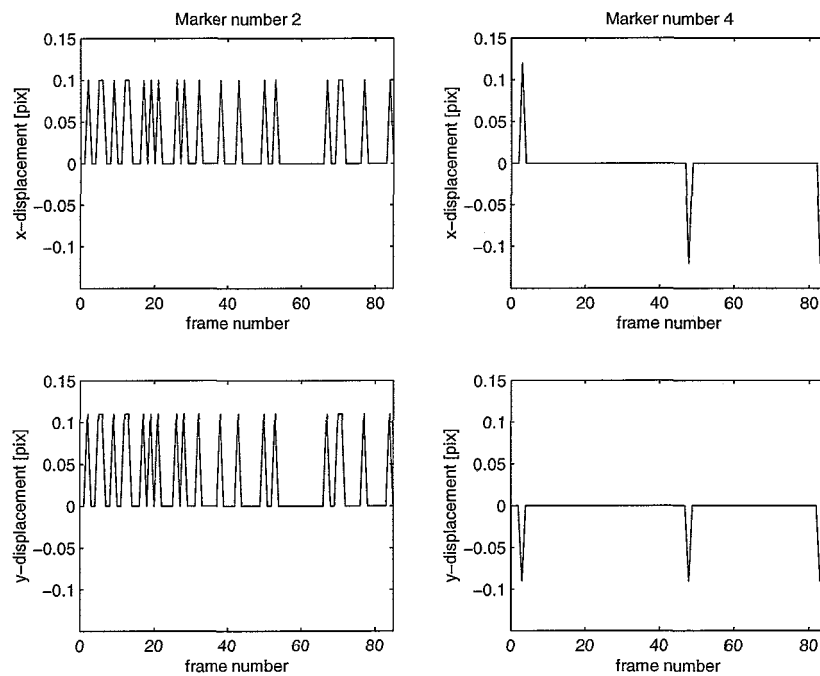
Figure C.2: Two typical characteristics of marker positioning by the data processing software
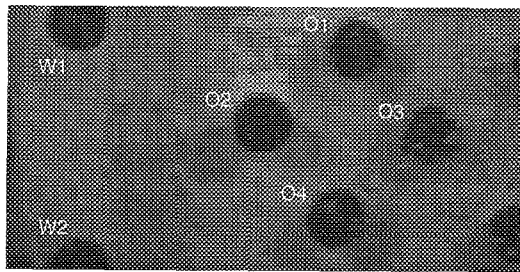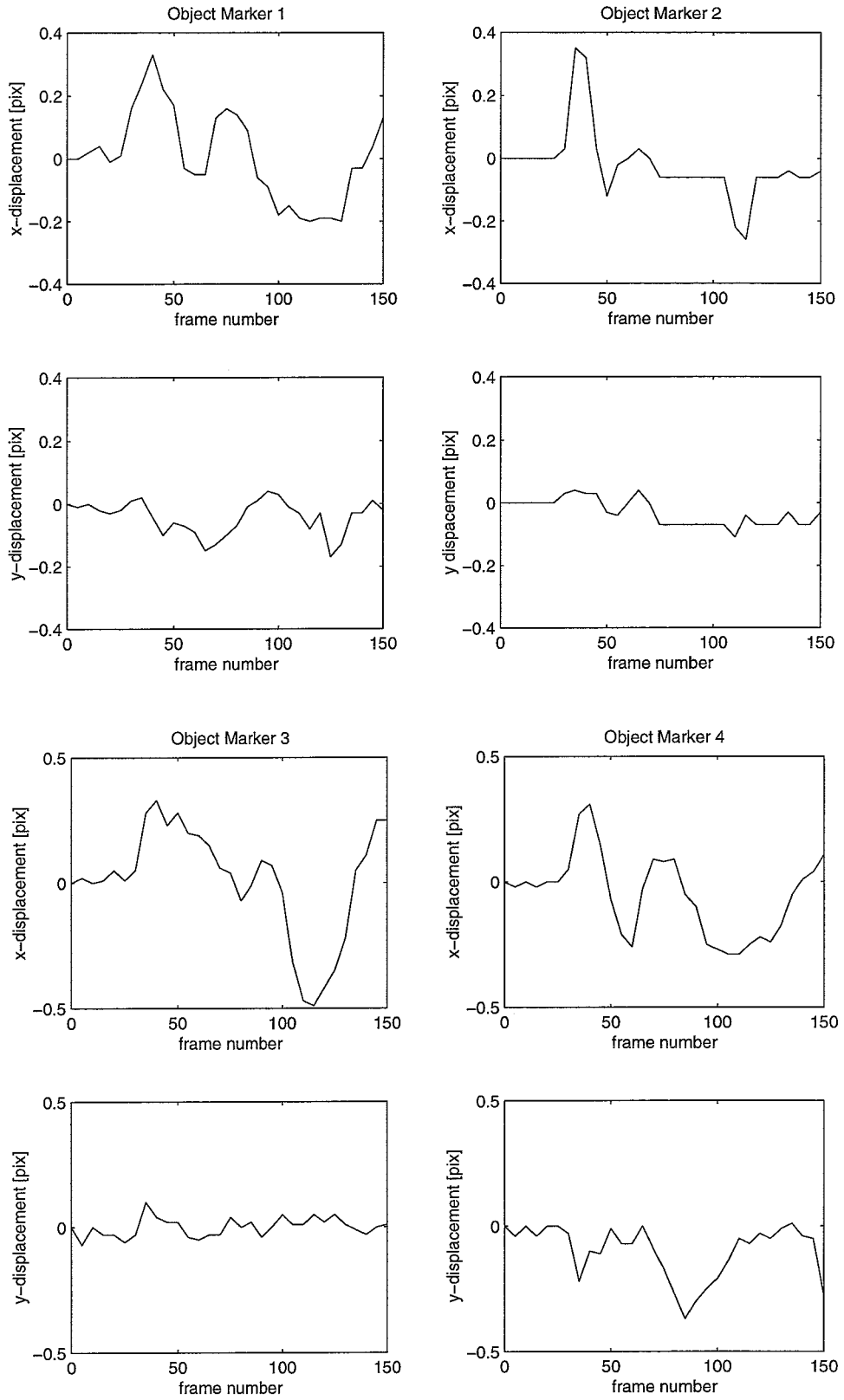
Appendix D

Surface Waves

Figure D.1: The area of the cup that was monitored during impact (frame size: 128×64 pixels)
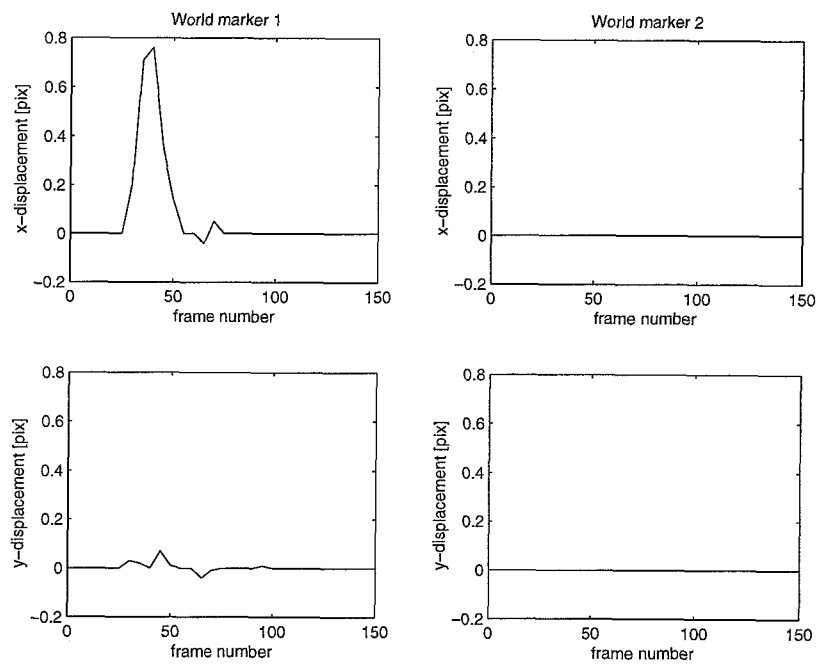
Figure D.2: World marker displacement

Figure D.3: Object marker displacement

32

Appendix E

Roersma's results
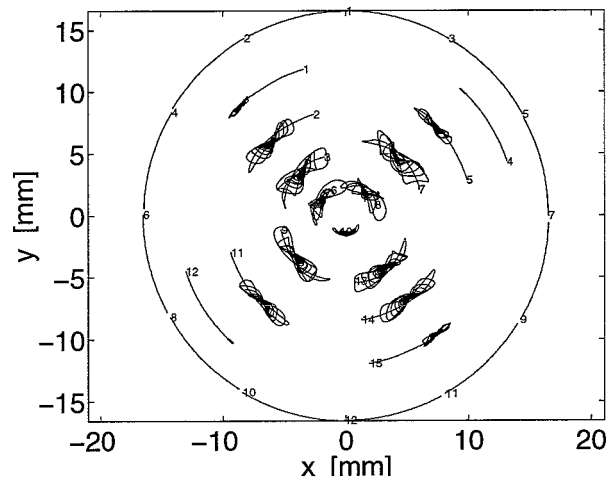
Figure E.1: Object and world marker trajectories, marker number at starting point, from [6]
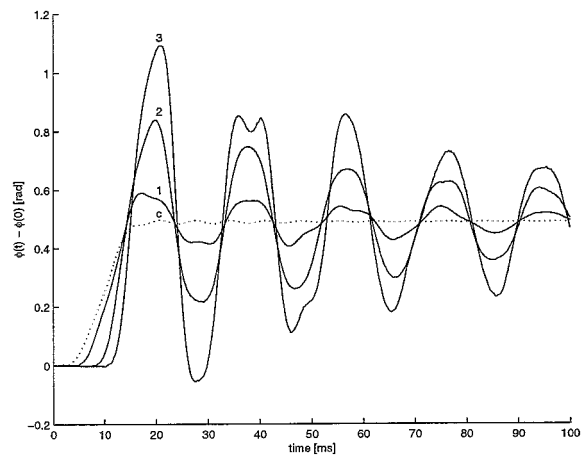
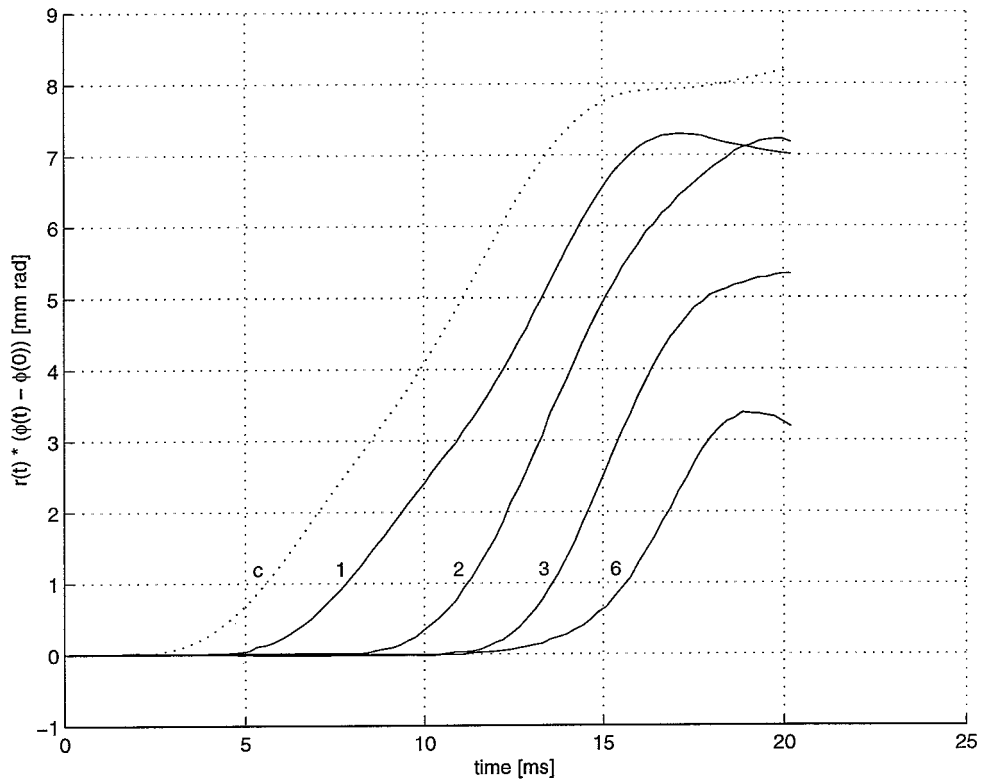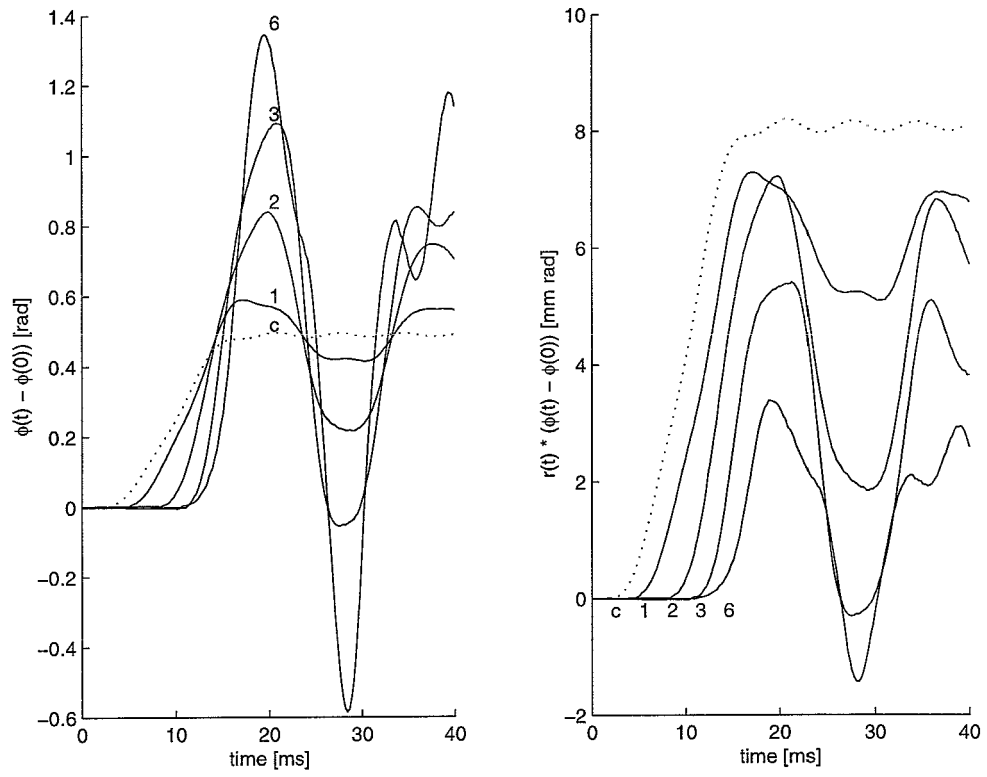**Figure E.2:** Rotation of object markers 1, 2 and 3 and cup, from [6]

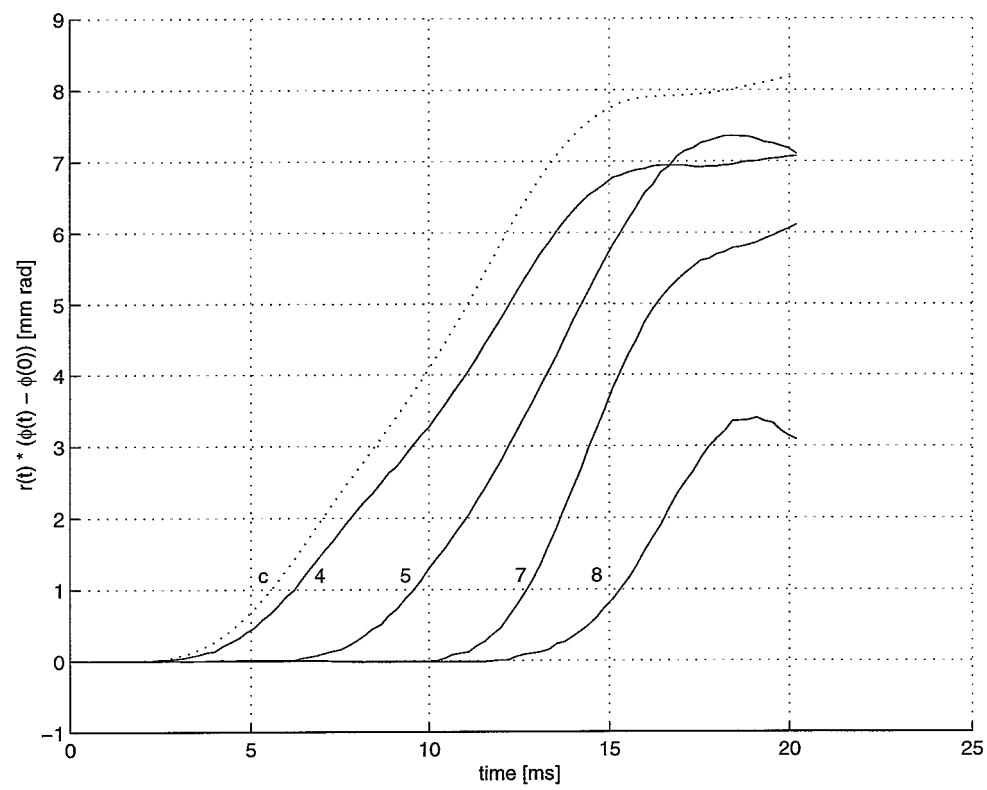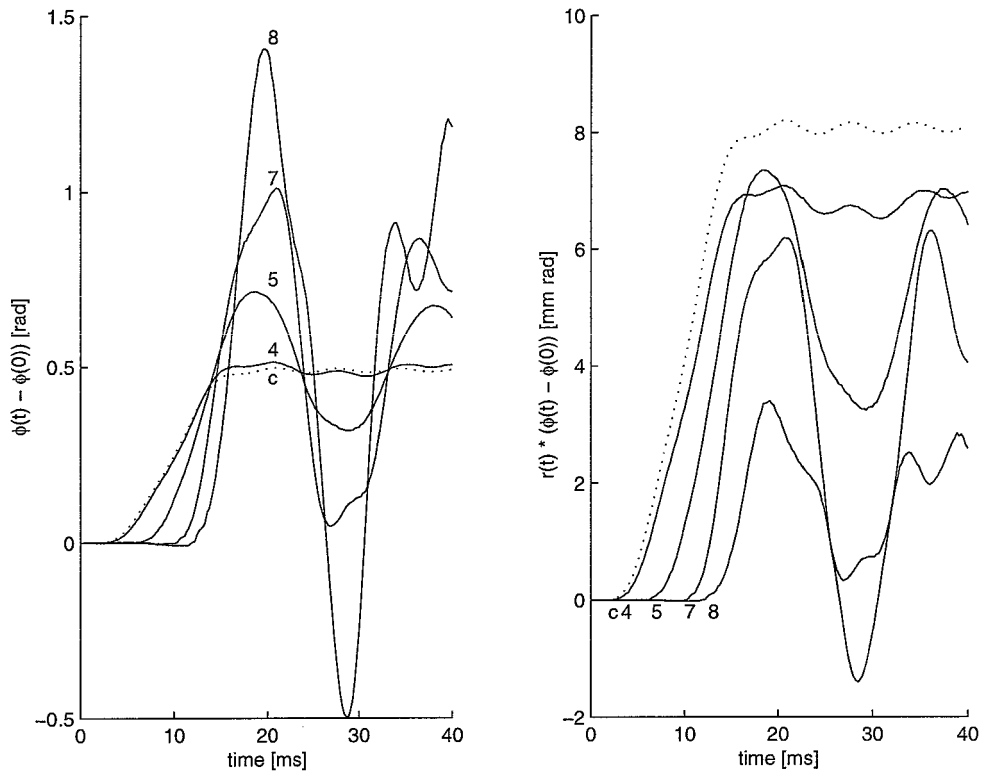**Figure E.3:** Some operations to get a clearer view of surface wave propagation

Figure E.4: Another sample from the same experiment